YU ISSN 0015—3206
FZKAAA 21 (2) 155 (1989)

CHAOS IN THE CONSTRAINED RESONANT SYSTEM

EDVARD GOVEKAR and IGOR GRABEC

Faculty of Mechanical Engineering, University E. Kardelj, p. p. 394, 61 000 Ljubljana, Yugoslavia

Received 8 September 1988

Revised manuscript received 27 February 1989

UDC 534.37

Original scientific paper

The article presents computer simulation of a harmonically forced, damped mechanical oscillator in which the motion is restricted on one side of the equilibrium position by a fixed wall. Due to elastic impacts with the wall, chaotic movement results if the system dissipation is low. With increasing driving amplitude, the transition from harmonic to chaotic, and further to nonlinear periodic motion is observed. The corresponding changes of the attractor are shown by its projections onto the $(X, \dot{X})$ plane. They are characterized by the Poincaré section and correlation dimension. The properties of typical oscillations are represented by the spectral distributions.

1. Introduction

In order to prevent large amplitude oscillations in mechanical structures the limiters of displacements are often applied. The influence of a limiter and other restoring forces is generally represented by a nonlinear function in dynamics equations of the corresponding system. Anharmonic oscillations can therefore be expected and the question arises: what kind of motion develops under given conditions and how can it be characterized?

The impact force problems have already been extensively studied in relation to the description of particle movements colliding with oscillating walls[1]. Beside these, oscillations of various restricted resonant systems have been described[2-4].

Common to all the models is the fact that in addition to anharmonic oscillations, chaotic movements can also be caused by the influence of limiters. The purpose of this article is to show that even the most simple restricted mechanical oscillator, composed of a mass-spring-dashpot placed in front of a fixed wall, also exhibits the same properties with increasing amplitude of periodical forcing.

The dynamic equations of the physical model are represented in the next section. The influence of the system parameters on the dynamics, and especially on the chaotic behaviour, are then analyzed in the third section while some possible practical applications are mentioned in the conclusion.

The dynamical model

The scheme of the system is shown in Fig. 1. A mass m is attached by a linear spring of stiffness k and a linear dashpot with damping factor b to a foundation oscillating according to the rule:

$$x_e(t) = x_0 \cdot \sin(\Omega \cdot t). \tag{1}$$

The limiter of motion is displaced by x_l from the equilibrium position of the mass.

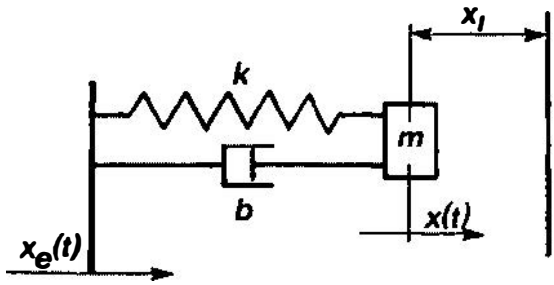

Fig. 1. Scheme of a constrained resonant system.

The complete influence of the linear spring and the limiter is described by the force:

$$F(x) = k \cdot (x - x_e) + f_l(x). \tag{2}$$

In this equation x represents the absolute displacement of the mass m from the equilibrium position and $f_l(x)$ denotes the influence of the limiter expressible by:

$$f_l(x) = \begin{cases} 0 & \text{if } x < x_l \\ \infty & \text{if } x \geq x_l. \end{cases}$$

Here the dot denotes differentiation with respect to dimensionless time τ and the following notation are introduced: $F(X) = (k \cdot x + f_l)/(k \cdot x_l)$, $\omega = \Omega \cdot (m/k)^{1/2}$, and

$$C \cdot \sin(\omega \cdot \tau + \varphi) = \alpha \cdot \sin(\omega \cdot \tau) + 2 \cdot \beta \cdot \omega \cdot \alpha \cdot \cos(\omega \cdot \tau).$$

The nonlinear characteristic of the restoring force F is shown in Fig. 2. By the nondimensional displacement $X = x/x_l$ and nondimensional time $\tau = (k/m)^{1/2} \cdot t$ the equation of motion can be written in the form:

$$\ddot{X} + 2 \cdot \beta \cdot \dot{X} + F(X) = C \cdot \sin(\omega \cdot \tau + \varphi). \tag{3}$$

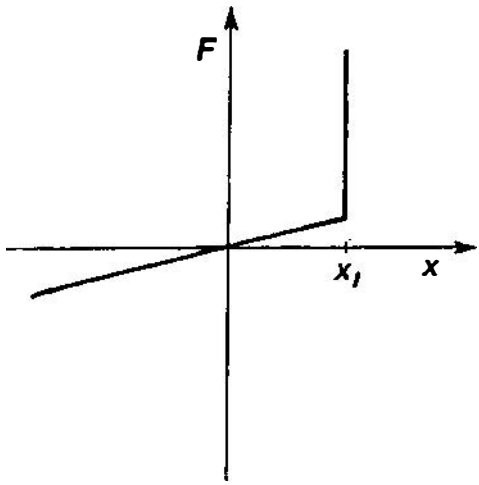

Fig. 2. Nonlinear system characteristics.

The parameters $\beta = b/(2 \cdot (k \cdot m)^{1/2})$ and $\alpha = x_0/x_l$ denote the damping coefficient and dimensionless forcing amplitude. Due to the singularity of the function $f_l(x)$ its analytical description is not suitable for further treatment. The effect of the limiter is to reverse the mass velocity during impact. This can be generally described by the impact rule:

$$\dot{X}(\tau^+) = -r \cdot \dot{X}(\tau^-), \tag{4}$$

which must be taken into account at $X(\tau) = 1$. In Eq. (4) the reflection coefficient r describes the dissipation of the energy due to the impact.

With such a description of the limiter influence, the analysis of motion can be divided into two parts. In the first part, the motion of the mass m between two successive impacts is described by the equation of the linear oscillator:

$$\ddot{X} + 2 \cdot \beta \cdot \dot{X} + X = C \cdot \sin(\omega \cdot \tau + \varphi); \qquad \tau \neq \tau_n, \tag{5}$$

while in the second part the impact of the mass against the fixed wall at the moment $\tau = \tau_n$ is described by Eq. (4).

The particular solution of Eq. (5) in the time interval between two impacts can be expressed in an analytical form including trigonometric and exponential functions. The impact time τ_n can be obtained from it and the condition $X(\tau) = 1$, which altogether lead to a transcendental equation solvable only numerically. It

was found that a solution can be more efficiently found if Eq. (5) is numerically solved by the Runge-Kutta method of the fourth order in the interval between the two impacts and the impact time τ_n is determined by the numerical method of bisection. The starting velocity conditions in a new interval are then expressible by Eq. (4).

3. *Properties of the constrained resonant oscillations*

Typical examples of possible motions of the mass m are shown in Fig. 3. The records obtained at different values of the parameters (ω, α, β, r) represent harmonic (Fig. 3a), nonlinear periodic (Fig. 3b) and apparently chaotic motion (Fig.

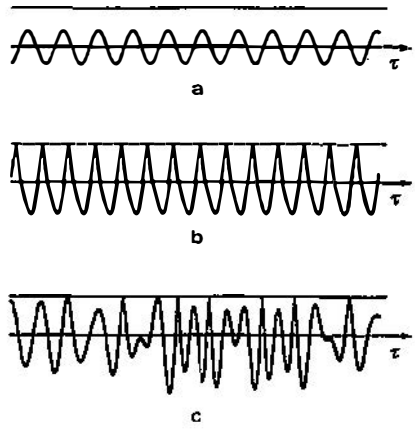

Fig. 3. Typical examples of oscillations.

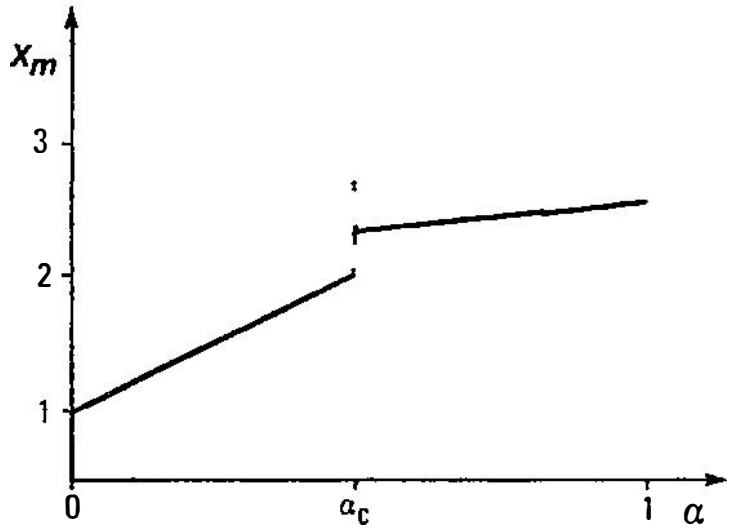

Fig. 4. The bifurcation diagram of motions for parameters ($\omega = 1.2$, $\beta = 0.1$, $r = 0.98$).

3c). In order to make posible graphical presentation of the influence of parameters on the type of motion, we describe each record by the series of maximal distances X_m from the limiter corresponding to the minima of the record. The dependence of these values on the parameter under consideration is then represented in the bifurcation diagram. When the system oscillates harmonically, only one value of distance $X_{m'1}$ is observed. At a given value of parameter α this corresponds to one point $(\alpha, X_{m'1})$ of the bifurcation diagram only. For irregular oscillations several distances $X_{m'i}$ are observed corresponding to different points $(\alpha, X_{m'i})$ at a certain

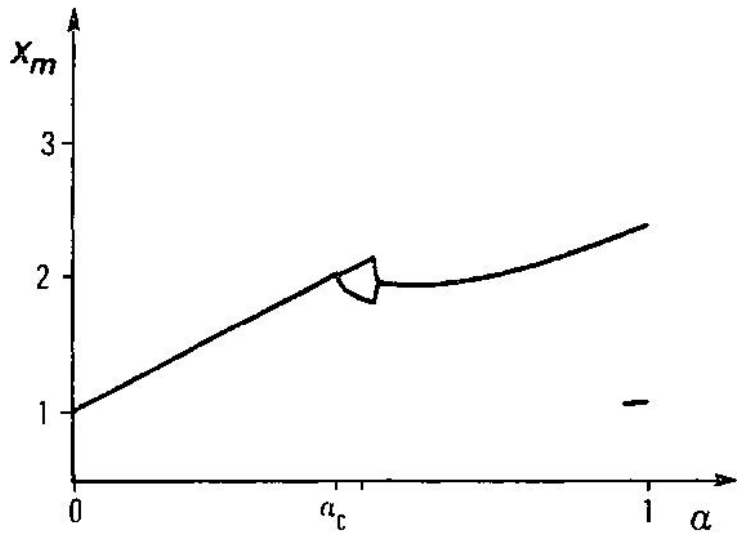

Fig. 5. The bifurcation diagram of motions for parameters ($\omega = 0.8$, $\beta = 0.2$, $r = 0.98$).

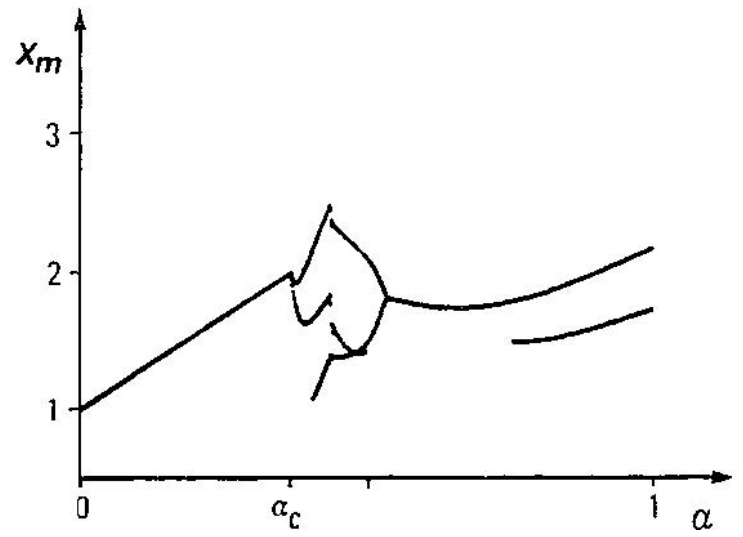

Fig. 6. The bifurcation diagram of motions for parameters ($\omega = 0.8$, $\beta = 0.05$, $r = 0.98$).

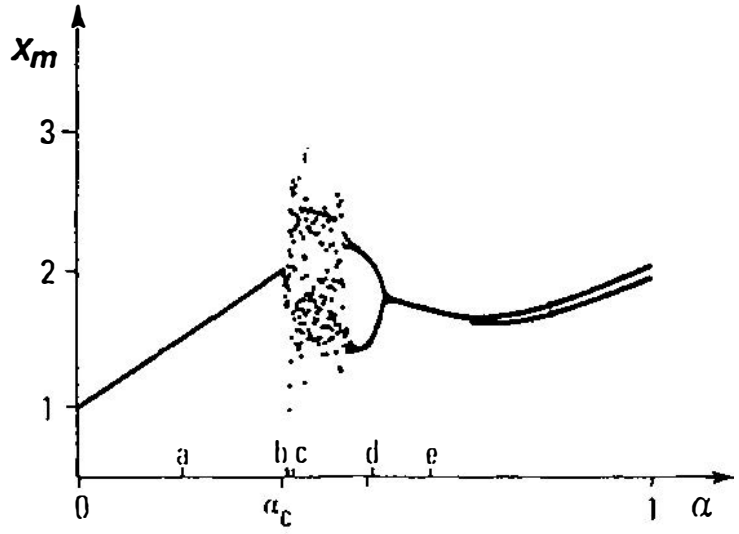

Fig. 7. The bifurcation diagram of motions for parameters ($\omega = 0.8$, $\beta = 0.005$, $r = 0.98$).

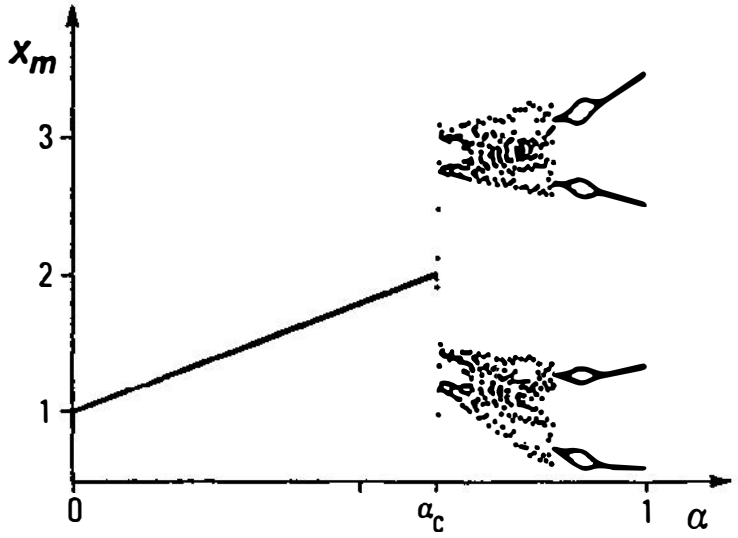

Fig. 8. The bifurcation diagram of motions for parameters ($\omega = 0.6$, $\beta = 0.005$, $r = 0.5$).

value of parameter α. Figs. 4—8 show the dependence of X_m on forcing amplitude α at various characteristic sets of other parameters (ω, β, r). At weak forcing, corresponding to low values of α, harmonic oscillations always take place, which correspond to one line in the bifurcation diagram. With an increasing forcing amplitude α, the oscillation amplitude grows and at a certain critical value α_c the impacts change the character of the movement. This can cause the bifurcation of the characteristic curve into two or more branches (Figs. 5—8). Periodic anharmonic oscillations

correspond to a finite number of branches while in the case of the chaotic movement, branches are continuously distributed over certain intervals.

Figs. 4—8 show typical examples of bifurcation diagrams which are observed at various combinations of characteristic parameters. Fig. 4 corresponds to the case where the impacts just cause a transition from harmonic to anharmonic periodic oscillations. Such diagrams are generally obtained at high system dissipation. Fig. 5 shows a second type of bifurcation diagram corresponding to harmonic and anharmonic oscillations only. The impacts first cause bifurcation into two branches, which afterwards recollapse into one branch. At a very high forcing amplitude, an additional abrupt bifurcation into two branches takes place. In the first bifurcation the interval between both branches grows continuously with increasing forcing while in the second one the growth is stepwise in spite of high damping. This observation shows that the complete mechanism of bifurcations is rather complex and can not be explained by the existing simple models[5,6]. This complexity is still emphasized when the system dissipation is decreased. In the surrounding of the first bifurcation point ever more bifurcation branches occur (Fig. 6), which later on leads to a chaotic state (Fig. 7). The structure of the bifurcation diagram in the chaotic state depends on the system parameters, as is observable from Figs. 7 and 8. It was found that the tendency to irregular motion generally increases with decreasing dissipation of the system.

The bifurcation diagrams indicate several possible modes of oscillation. In order to represent their properties we apply the spectra of the signals obtained

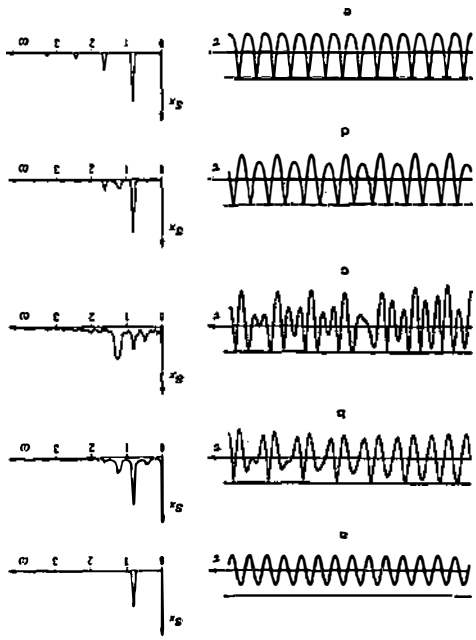

Fig. 9. The records of oscillations corresponding to the bifurcation diagram of Fig. 4 and the related spectra.

during the forming bifurcation diagram in Fig. 7. The signals and the corresponding spectra $S_x(\omega)$ are shown in Figs. 9a—9e for the values of parameter α indicated in Fig. 7. The first diagram (Fig. 9a), corresponds to harmonic oscillations without impacts. Diagram (Fig. 9b) represents the transition from harmonic to anharmonic movement. It is characteristic that the onset of impact is accompanied by the generation of sub- and higher-harmonic peaks. For the apparently chaotic movement a continuous spectrum (Fig. 9c) is characteristic. However, the free motion of the oscillator during the successive impacts is still present and causes distinct spectral peaks in this case as well. Anharmonic oscillations taking place above the chaotic region are again characterized by discrete spectra (Figs. 9d—9e). Diagram (Fig. 9b) indicates with its subharmonic peak that the transition from harmonic to chaotic oscillations proceeds over period doubling although the mechanism is not so simple as in the Feingenbaum scheme[5]. Similarly the collapse from chaotic to anharmonic oscillations (inverse bifurcation) proceeds over the disappearance of subharmonic peaks as indicated by Figs. 9d—9e.

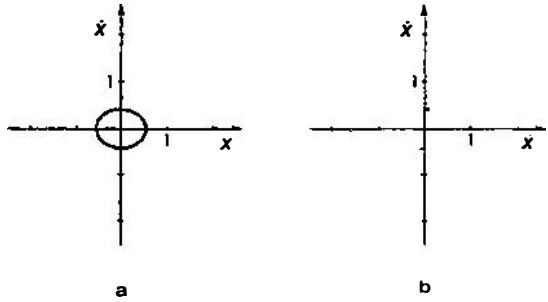

Fig. 10. The projection of the attractor onto the $(X, \dot{X})$ plane and the corresponding Poincaré section for parameters ($\omega = 0.8$, $\beta = 0.005$, $r = 0.98$, $\alpha = 0.19$) corresponding to point a in the bifurcation diagram of Fig. 8.

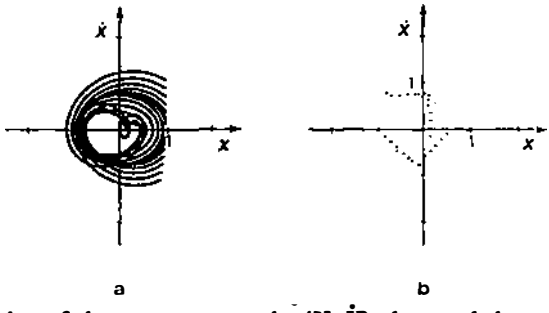

Fig. 11. The projection of the attractor onto the $(X, \dot{X})$ plane and the corresponding Poincaré section for parameters ($\omega = 0.8$, $\beta = 0.005$, $r = 0.98$, $\alpha = 0.35$) corresponding to point b in the bifurcation diagram of Fig. 8.

The motion of the oscillator can be represented in three-dimensional phase space if beside X and $\dot{X}$ the dimensionless force $X_e = \alpha \cdot \sin(\omega \cdot \tau)$ is introduced as the third component. The system trajectories in this phase space take place on

an attractor, the properties of which were demonstrated by projections onto the $(X, \dot{X})$ plane and by the Poincaré section obtained by the same plane, $(X_e = 0)$. For typical examples of the motion presented in Figs. 9a—9e the projections onto the $(X, \dot{X})$ plane and Poincaré sections are shown in Figs. 10—14. The change of the attractor structure is visible in these figures. First the change from the simple limit cycle of Fig. 10 into the quasi periodic attractor of Fig. 11 is observed. At this transition the Poincaré section changes from two to many points indicating one-dimensional distribution. The transition to chaotic motion is accompanied by the expansion of the attractor in the phase space into a bandlike form (Fig. 12a). The strange character of the attractor is indicated by the two-dimensional distribution of the Poincaré section (Fig. 12b). The collapse of the attractor back to the limit cycle caused by increasing forcing is then demonstrated by Figs. 13 and 14, which

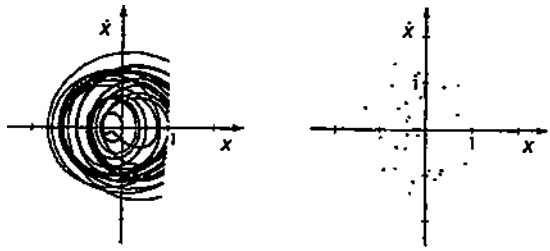

Fig. 12. The projection of the attractor onto the $(X, \dot{X})$ plane and the corresponding Poincaré section for parameters ($\omega = 0.8$, $\beta = 0.005$, $r = 0.98$, $\alpha = 0.37$) corresponding to point c in the bifurcation diagram of Fig. 8.

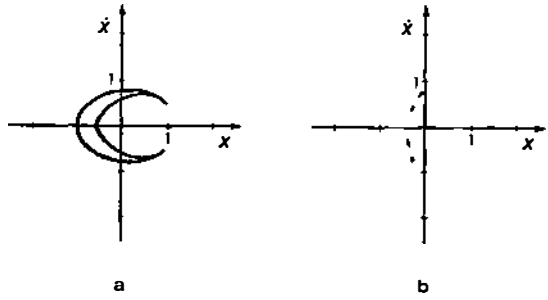

Fig. 13. The projection of the attractor onto the $(X, \dot{X})$ plane and the corresponding Poincaré section for parameters ($\omega = 0.8$, $\beta = 0.005$, $r = 0.98$, $\alpha = 0.51$) corresponding to point d in the bifurcation diagram of Fig. 8.

clearly demonstrate the transition from a two- to a one-period cycle. For the strange attractor the average divergence of the trajectories is generally characteristic. In the case of the attractor presented in Fig. 12 this property is indicated in Fig. 15, which shows, after eight impacts, two trajectories starting from slightly different initial conditions. Due to this divergence, the correlation function of the displace-

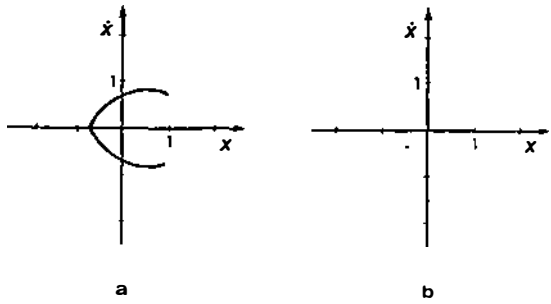

Fig. 14. The projection of the attractor onto the $(X, \dot{X})$ plane and the corresponding Poincaré section for parameters ($\omega = 0.8$, $\beta = 0.005$, $r = 0.98$, $\alpha = 0.62$) corresponding to point e in the bifurcation diagram of Fig. 8.

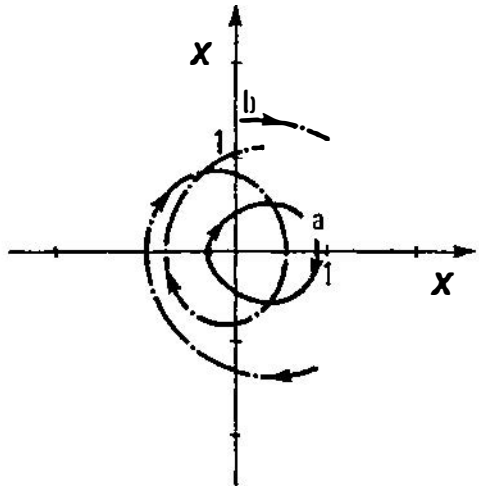

Fig. 15. Two trajectories stemming from very close initial conditions on the strange attractor after eight impacts.

TABLE 1.

α	0.19	0.35	0.37	0.51	0.62
D_2	1.08	2.07	2.62	1.13	1.05

Correlation dimension D_2 dependence on the forcing amplitude α for parameters ($\omega = 0.8$, $\beta = 0.005$, $r = 0.98$).

ment in the chaotic regime decays with time[7]. For the characterization of the attractor changes, the correlation dimension D_2 was applied. Its dependence on the forcing amplitude is shown in Table 1. With the transition from limit cycle to strange attractor the correlation dimension changes from 1 to 2.6. The fractal dimension confirms the strange character of the chaotic attractor.

4. Conclusion

In this paper we have shown that a simple constrained driven resonant system exhibits very complex dynamical behaviour. At low and medium damping a transition from harmonic through chaotic to anharmonic oscillations can be caused by increasing the forcing amplitude. As in many other dynamical systems, increased damping generally diminishes the possibility of the onset of chaotic movement. This fact can be applied to avoid undesirable irregular behaviour of various mechanical devices like relays, electric switches, printers, etc. It is important that there are two parameters by which dissipation can be controlled, i. e. the dashpot damping and the reflection coefficient. If high amplitude movement is wanted, the dashpot damping should generally below, so the only possibility of avoiding irregular movement is to increase the dissipation at the impact.

References

1) A. J. Lichtenberg and M. A. Lieberman, *Regular and Stohastic Motion*; Springer Verlag, New York, 1983;
2) S. W. Shaw and P. J. Holmes, Journal of Sound and Vibration **90** (1983) 129;
3) S. W. Shaw and P. J. Holmes, Journal of Applied Mechanics **51** (1983) 623;
4) J. M. Thompson and R. Ghaffari, Physics Letters **91 A** (1982) 5;
5) H. G. Shuster, *Deterministic Chaos, An Introduction*; Physik Verlag, Weinheim, 1984;
6) F. C. Moon, *Chaotic Vibrations, An Introduction for Applied Scientists and Engineers*, John Wiley and Sons, 1987;
7) E. Govekar, B. E. Thesis, No. 3550; Department of Mechanical Engineering, University E. Kardelj Ljubljana, 1987.

KAOTIČNO GIBANJE OMEJENEGA RESONANČNEGA SISTEMA

EDVARD GOVEKAR in IGOR GRABEC

Fakulteta za strojništvo, Univerza E. Kardelj, p. p. 394, 61000 Ljubljana

UDK 534.37

Originalni znanstveni rad

Prispevek obravnava računalniško simulacijo enostransko omejenega, dušenega resonančnega nihanja mase na prožni vijačni vzmeti. Pri majhnih dušenjih sistema se zaradi elastičnih trkov mase z omejevalnikom gibanja pojavi prehod v kaotično gibanje. Z naraščanjem amplitude vzbujanja je najprej viden prehod iz harmonskega v kaotično gibanje, nato pa prehod iz kaotičnega v nelinearno periodično gibanje. Pripadajoče spremembe atraktorja so prikazane s projekcijami atraktorja na ravnino $(X, \dot{X})$. Okarakterizirane so s Poincaré-jevo sekcijo in korelacijsko dimenzijo. Karakteristične oscilacije so predstavljene s pripadajočimi spektralnimi porazdelitvami.